Emergence of universal scaling in isotropic turbulence

Sualeh Khurshid, Diego A. Donzis, and Katepalli R. Sreenivasan

Emergence of universal scaling in isotropic turbulence

Sualeh Khurshid

Department of Mechanical Engineering, Massachusetts Institute of Technology and
Department of Aerospace Engineering, Texas A&M University

Diego A. Donzis

Department of Aerospace Engineering, Texas A&M University

Katepalli R. Sreenivasan

Department of Mechanical & Aerospace Engineering, Department of Physics,
Courant Institute of Mathematical Sciences, New York University

Universal properties of turbulence have been associated traditionally with very high Reynolds numbers, but recent work has shown that the onset of the power-laws in derivative statistics occurs at modest microscale Reynolds numbers of the order of 10, with the corresponding exponents being consistent with those for the inertial range structure functions at very high Reynolds numbers. In this paper we use well-resolved direct numerical simulations of homogeneous and isotropic turbulence to establish this result for a range of initial conditions with different forcing mechanisms. We also show that the moments of transverse velocity gradients possess larger scaling exponents than those of the longitudinal moments, confirming past results that the former are more intermittent than the latter.

I. BACKGROUND

Turbulence is characterized by strong amplitude fluctuations over spatial scales that range, nominally, from large scales $O(L)$ to dissipating small scales $O(\eta)$. A similar range of temporal scales exists as well. Within the classical turbulence phenomenology, large scales depend on the geometry of the flow, or the generation mechanism of turbulent fluctuations, while the small scales increasingly approach universal behavior as the scale-separation grows [1–6]. A measure of scale-separation in turbulent flows is the Reynolds number. The universality of small scales at high Reynolds numbers is an enduring notion in turbulence theory and forms the bedrock of most modelling approaches [1, 2, 6–9]. This view was formalized in Kolmogorov's seminal work (K41) and its subsequent modifications (see [4–6]), which characterize the statistical behavior of fluctuations at different scales, in particular a Reynolds-number-independent state of the inertial range ($L \gg r \gg \eta$). Universality of small scales is expected to manifest more rigorously at high Reynolds numbers, which has been the motivation for studying turbulence at ever increasing Reynolds numbers.

The theory itself does not provide guidance on how high a Reynolds number should be regarded as "high enough", but it is not uncommon to regard an R_λ of the order of a few hundred or more as necessary for the inertial scaling to appear [6, 10–17]. Here,

$$R_\lambda \equiv \sqrt{5/(3\langle\epsilon\rangle\nu)}u_{rms}^2,$$

where $\epsilon = 2\nu s_{ij}s_{ij}$ is the (instantaneous) energy dissipation rate, ν is the kinematic viscosity and u_{rms} is the root-mean-square fluctuating velocity; s_{ij} is the rate of strain given by $(\partial_i u_j + \partial_j u_i)/2$ using Einstein's summation convention and angular brackets indicate volume averages over an ensemble of realizations in time. However, recent work has shown that moments of the longitudinal velocity gradient, which characterizes small-scale activity, transitions to power-law scaling at much lower R_λ than expected from standard scaling arguments, with the same universal exponents that characterize high Reynolds numbers [18]. For fluctuations forced by Gaussian white noise at large scales, it was also shown that the transition from the Gaussian state to the scaling state occurs at very low Reynolds number, $R_\lambda = O(10)$ [19, 20].

II. MOTIVATIONS AND GOALS

This result, if true, is important because it implies that the inertial range properties are incipient even when the actual inertial range does not exist in its full splendor. It is unclear from previous studies whether the onset of power-law scaling, as well as its exponents, depend on the particular large-scale forcing used to generate turbulence. If the results are independent of the forcing, they provide added credibility for the notion of universal scaling at low R_λ. So we drive the system at large scale using different forcing schemes and test the universality of the transition of velocity gradients and their scaling as discussed in [19, 20]. Specifically, Yakhot & Donzis [19] showed that even-order moments of longitudinal velocity gradients

$$M_{2n}^{||} = \langle(\partial_\alpha u_\alpha)^{2n}\rangle/\langle(\partial_\alpha u_\alpha)^2\rangle^n \tag{1}$$

exhibit Gaussian behavior below a critical $R_{\lambda,tr}(n)$, beyond which an order-dependent power-law scaling is observed—that is, $M_{2n}^{||} \propto R_\lambda^{2d_n}$ for $R_\lambda > R_{\lambda,tr}(n)$. The transition Reynolds number $R_{\lambda,tr}(n)$ depends on the moment order as $R_{\lambda,tr}(n) \propto \hat{R}_{\lambda,tr}^{\frac{2nd_n}{2d_n+3}}$, where the order-independent Reynolds number $\hat{R}_{\lambda,tr}(n) \equiv$
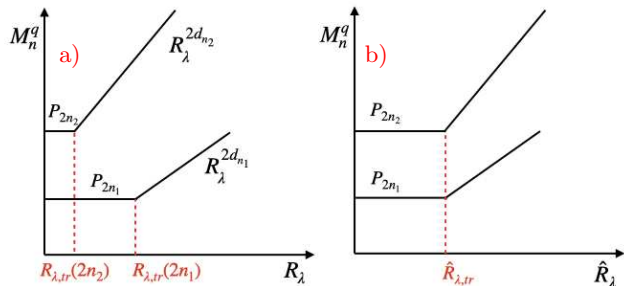
FIG. 1. Sketch depicting the transition from the low-R_λ Gaussian asymptote to power-law scaling for moments of two different orders ($n_2 > n_1$) with respect to (a) the standard Reynolds number, and (b) order-independent Reynolds number.

$L^2 \langle (\partial_\alpha u_\alpha)^n \rangle^{\frac{1}{n}} / \nu$ is of order 10, though slowly decreasing with increasing n [20]. Higher-order moments transition to power-laws at lower Reynolds numbers, presumably because they capture stronger fluctuations (which are rare). This is sketched in Fig. 1. If the low-R_λ asymptote (denoted by P_n) as well as the transition Reynolds number are known, the (high-R_λ) scaling exponents can be deduced simply by matching the two asymptotes at the transition Reynolds number (Fig. 1). Indeed, the scaling exponents so obtained are

$$d_n = -\frac{2n \log(\hat{R}_{\lambda,tr}) - 3nC' + 2 \log(P_{2n})}{4C'} +$$
$$\frac{\sqrt{(2n \log(\hat{R}_{\lambda,tr}) + 3nC' - 2 \log(P_{2n}))^2 + 24nC' \log(P_{2n})}}{4C'} \tag{2}$$

where $C' = \log(C)$ and C is a constant of about 90 [19, 20]. As already stated, these derivative exponents are consistent with the structure function exponents in the inertial range [18], obtained from experiments and simulations at high Reynolds numbers. Thus, although there is no inertial range near Reynolds numbers marking the transition [8, 20–22], its signature is apparently present already at very modest R_λ.

A related question is whether longitudinal and transverse gradients scale differently [13, 23–26], which we assess here within the context of the transition from Gaussian fluctuations to those with power-law scaling. We also study gradient-dependent quantities such as the enstrophy density $\Omega \equiv \omega_i \omega_i$, where $\boldsymbol{\omega} = \nabla \times \boldsymbol{u}$ is vorticity, as well as energy dissipation, $\epsilon = 2\nu s_{i,j} s_{i,j}$. Enstrophy is more intermittent than dissipation [24], but their mean values are related as $\langle \epsilon \rangle = \nu \langle \Omega \rangle$. The scaling of enstrophy is important for understanding finite-time blow-up and uniqueness problems of fluid-dynamical equations [27, 28]. We relate the new findings for enstrophy to the recent work on the transition in the nature of dissipation [18, 29–31].

III. DIRECT NUMERICAL SIMULATIONS

We study homogeneous, isotropic turbulence in a triply periodic domain governed by forcing the incompressible Navier-Stokes equations

$$\frac{\partial u_i}{\partial x_i} = 0 \tag{3}$$

$$\frac{\partial u_i}{\partial t} + u_j \frac{\partial u_i}{\partial x_j} = -\frac{1}{\rho} \frac{\partial p}{\partial x_i} + \nu \frac{\partial^2 u_i}{\partial x_i^2} + f_i \tag{4}$$

where u_i is the velocity component in the x_i direction, and p and ν are pressure and viscosity, respectively. The forcing term f_i adds energy into the system to balance dissipation and achieve a statistically stationary state. Details of different forcing mechanisms are described next and summarized in table I.

Gaussian forcing is widely used in the literature [19, 20, 26, 32]. We use three different forcing schemes $\boldsymbol{f}$. First, we modify the forcing such that forcing amplitudes have an exponential distribution with a random phase, and term this as exponential forcing. Both Gaussian and exponential forcing schemes are white in time. Second, we use the so-called linear forcing in which the forcing is proportional to the velocity field, that is, $\boldsymbol{f} = A\boldsymbol{u}$ where A is a constant. This forcing has qualitative resemblance to that experienced in a turbulent flow subjected to mean shear [30, 33–36]. As with the stochastic forcing this forcing is applied at low wavenumbers [15, 34, 35]. Third, we implemented a modification by forcing the momentum equations with vorticity (i.e. $\boldsymbol{f} = A\boldsymbol{\omega}$), which is intermittent unlike the velocity, but do not present these results here. We note that all the forcing functions are limited to low wavenumbers and exhibit nearly Gaussian statistics in physical space. However, their dynamics differ qualitatively.

Equations (3) and (4) are solved using a standard psuedospectral method [37, 38] with very good small scale resolution $k_{max}\eta \gtrsim 3$. The time step is evolved using a second-order Runge-Kutta algorithm with a constant time step such that the Courant-Friedrichs-Lewy condition ($CFL = |u_{max}|\Delta t/\Delta x$) remains below 0.3. These high resolutions allow us to reliably measure higher order moments of velocity gradients [39, 40]. All simulations are initialized with the same velocity field. To guarantee convergence, we record *at least* 50 large scale eddy turnover times in the stationary state. Gradient moments are computed using at least 100 snapshots separated by about half an eddy turnover time. We have verified that the skewness in the scaling range is -0.5, the ratio of longitudinal and transverse integral length scales is 2, and that the kinematic constraint between the longitudinal correlation function $f(r) = \langle u_\alpha(x_\alpha)u_\alpha(x_\alpha + r)\rangle/\langle u_\alpha^2\rangle$ and the transverse correlation function $g(r) = \langle u_\beta(x_\alpha)u_\beta(x_\alpha+r)\rangle/\langle u_\beta^2\rangle$, β being orthogonal to α, namely $g(r) = f(r) + (r/2)f'(r)$, is satisfied accurately.

TABLE I. Details of forcing. Gauss and Exponential are stochastic forcing schemes that are white in time and follow Gaussian and exponential distributions, respectively. A is a constant. The maximum and minimum small-scale resolution in units of $k\eta$ are 60 and 3, depending on R_λ, for all types of forcing.

Type	Forcing band
Gauss	$0 < k \leq 2$
Exponential	$0 < k \leq 2$
$u(k)$	$5 \leq k \leq 6$
$\omega(k)$	$5 \leq k \leq 6$

IV. ASYMPTOTIC STATES AND SCALING

We are interested in the moments of the derivative q in the form $M_n^q = \langle q^n \rangle / \langle q \rangle^n$ where n is the order of the moment. The moments of longitudinal velocity gradients from simulations with different forcing mechanisms are shown in Fig. 2a. They show a composite of a low-R_λ Gaussian asymptote (dashed horizontal lines) and a transition to anomalous scaling (dashed lines showing power-laws). The Gaussian asymptote for low-R_λ, the onset of transition, and the exponents of power-law regime are all essentially independent of forcing. The scaling for longitudinal gradients can be accurately fitted by the analytical derivation of power laws in [20] (dashed lines) assuming that the low-R_λ moments are Gaussian and a universal transition occurs at $\hat{R}_{\lambda,tr} = 9.89$ (Eq. (2)). Open circles for Gaussian forcing follow the earlier result [19, 20] quite well. Note that the power-law behavior is traditionally expected at much higher R_λ than those found here.

In Fig. 2b, we have plotted the moments of transverse velocity gradients (symbols) along with the scaling predicted from Eq. (2) for longitudinal gradients (dashed lines). As for the longitudinal gradients, the transverse velocity gradient moments exhibit a low-R_λ Gaussian asymptote and transition to power-law scaling beyond a small value of R_λ, and are also independent of the large-scale forcing mechanism. However, two differences become clear when Figs. 2 a and b are compared: the transition for high-moments occurs at a lower R_λ than 10, and the moments of transverse gradients grow faster than longitudinal gradient moments, with this tendency increasing with increasing moment order. This is consistent with the claims of Refs. [13, 23, 25, 26, 41] that transverse gradients are more intermittent than the longitudinal. We emphasize that, while the scaling exponents for different gradients are different, the behavior of a given gradient is independent of forcing. The theory [20] allows for this possibility, so the constants in Eq. (2) depend on whether they refer to the longitudinal or transverse gradients.

To quantitatively support the observations just made, we now compute the transition Reynolds number as well
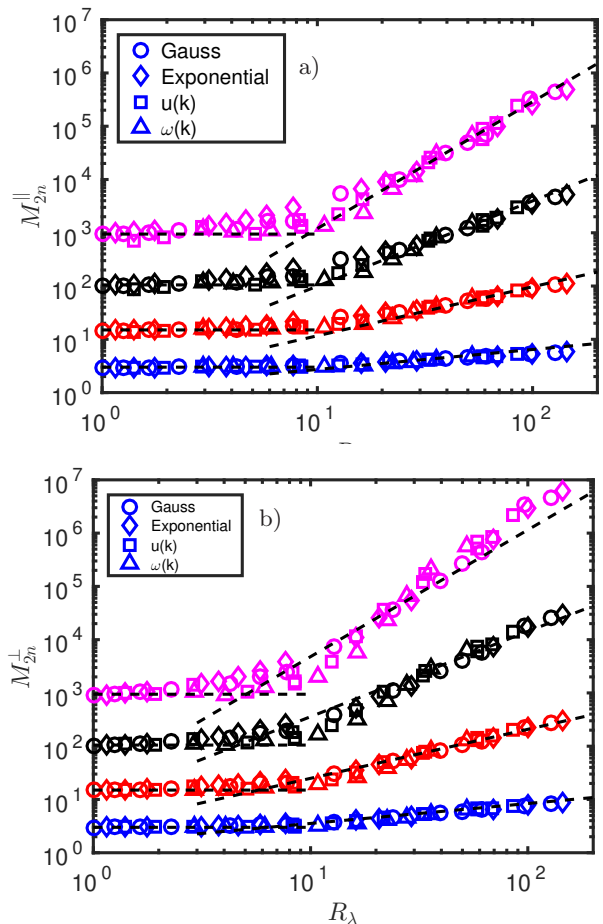

FIG. 2. Moments of (a) longitudinal and (b) transverse velocity gradients for $2n = 4$ (blue), 6 (red), 8 (black), and 10 (magenta). The horizontal dashed lines correspond to Gaussian moments, and power-laws correspond to $R_\lambda^{2d_n}$ from [20] where the d_n are given by Eq. (2), with $\hat{R}_{\lambda,tr} = 9.89$. The transverse moments in (b) follow steeper power laws than the longitudinal moments in (a).

as exponents in the power-law regime. In the previous work [20], only the power-law part was used for fitting purposes but this method is sensitive to the fitting range [26]. We mitigate this problem by fitting the entire data by a single functional form for M_{2n}^q that captures both the low-R_λ asymptote and the power-law part. Such a procedure of using scaling functions, rather than the power-law part alone, is more reliable for obtaining scaling parameters [42]. Since we have no analytical guidance on the full details of the transition, we can pragmatically propose the following functional form that satisfies our requirements:

$$M_{2n}^q = C_{2n}^q + \alpha_{2n}^q C_{2n}^q \left(\frac{R_\lambda}{R_{\lambda,tr}(2n)} \right)^{\beta_{2n}^q}. \quad (5)$$

Here α_{2n}^q is expected to be of the order unity, and the other three fitting parameters are the low-R_λ asymptote C_{2n}^q, the transition Reynolds number $R_{\lambda,tr}(2n)$, and the

high-R_λ scaling exponent β_{2n}^q. Since α_{2n}^q and C_{2n}^q appear as a product, there are only three independent fitting parameters, so we rewrite the above form as

$$M_{2n}^q = C_{2n}^q \left(1 + \left(\frac{R_\lambda}{b_{2n}^q} \right)^{\beta_{2n}^q} \right), \tag{6}$$

where $b_{2n}^q = R_{\lambda,tr}(2n)/(\alpha_{2n}^q)^{1/\beta_{2n}^q}$ for a given quantity q and order $2n$. Stable and accurate fits are possible if the data extend at least up to $R_\lambda = O(100)$.

The low-R_λ asymptotes for the moments ($= C_{2n}^q$) so obtained are plotted in Fig. 3a along with the appropriate Gaussian values (dashed line). The two are very close to each other for both longitudinal and transverse moments for all forcing methods, consistent with the observation in Fig. 2. The parameter b_{2n}^q, which is proportional to the transition R_λ, decreases with increasing moment order, supporting the theoretical results of [19]. For the lowest order ($n = 2$), the values of b_{2n}^q are $O(10)$. Obtaining accurate values of b_{2n}^q at low orders is challenging because this parameter is essentially the intersection of the low-R_λ and high-R_λ asymptotes which, as seen in Fig. 2, become closer to being co-linear, making the problem ill-conditioned. For a given forcing, the transition R_λ is lower for transverse gradients (blue symbols) than for the longitudinal (red symbols). Although small differences exist for b_{2n}^q at a given n for different forcing methods, they are within statistical bounds. In Fig. 3e, the average values of of b_{2n}^q over all three forcing schemes clearly show the persistence of differences between transverse and longitudinal gradients.

The power-law exponent $\beta_{2n}^q = 2d_n^q$ is plotted in Fig. 3f for the three different forcing methods. Again, the scaling exponents are larger for transverse gradients. Those for longitudinal gradients are consistent with earlier measurements made in isotropic turbulence, turbulent channel, and Rayleigh-Bénard convection [18, 25, 26, 31, 43]. We also include Eq. (2) (dashed line) which fit the data with $\hat{R}_{\lambda,tr} = 9.89$ (red) and 2 (blue) for longitudinal and transverse gradients, respectively. Overall, the physical picture is that large transverse gradients acquire their high-R_λ asymptotic behavior at lower Reynolds number than longitudinal ones. The faster growth of transverse moments implies smaller scaling exponents of transverse structure functions in the inertial range. This result has recently been reported in [13] using data from $R_\lambda \gtrsim 650$, much larger than those reported here.

Yakhot & Donzis [20] allowed for different exponents for longitudinal and transverse gradients, but did not provide a physical reasoning. Recent work [8, 13] argues that high-order moments of velocity increments in the inertial range are decreasingly affected by pressure gradients, with two possible consequences. First, it leads to stronger fluctuations and a transition at a lower-R_λ for high-order moments. Second, the transverse fluctuations are even less susceptible to pressure effects, possibly leading to differences in power-law scaling between longitudinal and transverse gradients.
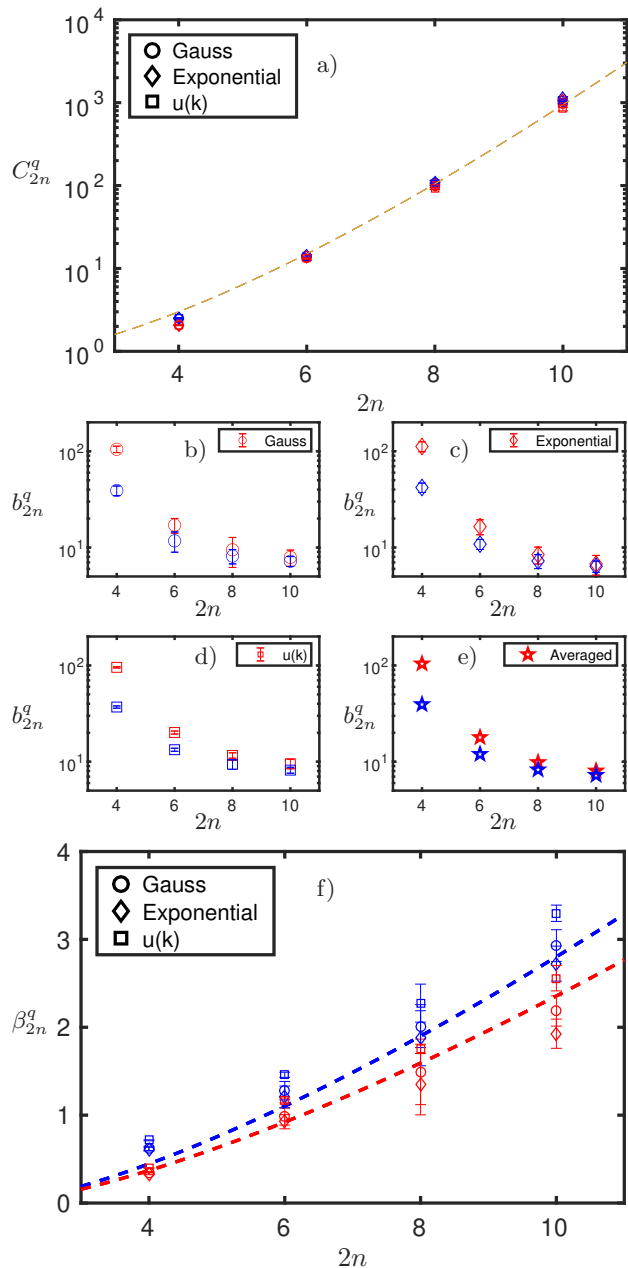

FIG. 3. Fit parameters for moments of longitudinal (red) and transverse (blue) velocity gradients. (a) The low-R_λ asymptotes, with the orange line denoting Gaussian moments. The constant $b_{2n}^q \propto R_\lambda^{tr}(n)$ are for the following forcing: (b) Gaussian (c) Exponential (d) u(k). (e) The mean values of b_{2n}^q for the three forcing schemes. (f) Scaling exponents for the different forcing methods. The red and blue lines correspond, respectively, to $\hat{R}_{\lambda,tr} = 9.89$ and 2 in Eq. (2). We generate 50 synthetic data points from a normal distribution with the same mean and variance as those observed for each realization of the DNS data. We then perform the fit with Eq. (6) on these datasets to generate a PDF for each fitting parameter. The 95% confidence interval for each parameter is generated from this PDF and shown in the figures. In many instances, the error bars are not much bigger than the symbol size.

Velocity gradients are important, in part, because they combine to form two quantities of particular interest in turbulence theory—the energy dissipation rate and enstrophy density ($\Omega_i = |\boldsymbol{\omega}|^2$ where $\boldsymbol{\omega}$ is the vorticity vector). While the moments of dissipation were shown [18, 26] to follow power-law scaling even at moderate R_λ, not much is known about enstrophy. We examine it here. In Fig. 4, we plot the moments of enstrophy (symbols) for different R_λ and forcing schemes. The dashed power-laws correspond to those observed in [18, 26, 31] and predicted by [19, 20]. For $R_\lambda \lesssim 10$, the asymptotic values correspond to moments of the χ^2 distribution with three degrees of freedom (dashed horizontal lines). The agreement towards the low-R_λ asymptote is expected as enstrophy is the sum of squares of three transverse gradients, each of which is Gaussian and independent of the other two, given the weak coupling expected at this low Reynolds numbers. Similarly dissipation exhibits χ^2 statistics with five degrees of freedom as the incompressibility condition constrains only five gradients to be independent. This feature is indeed observed in our data as well (not shown here). Similar to individual gradients, the transition to the anomalous regime for enstrophy appears to be independent of the details of forcing. We also note that scaling exponents for enstrophy are larger than those for dissipation (shown as dashed-line power laws in Fig. 4). Enstrophy moments grow faster than those of dissipation, increasingly so at higher orders. These observations are consistent with the available evidence at much higher R_λ that extreme events in enstrophy are more probable than in dissipation [23, 26, 39]. We thus conclude that high-R_λ behaviors for dissipation and enstrophy are also incipient at low Reynolds numbers $R_\lambda \sim O(10)$, which marks the transition.

V. CONCLUSIONS

We have shown here that anomalous scaling for velocity gradients and enstrophy emerges at $R_\lambda \sim O(10)$, much lower than traditionally expected, consistent with [19]. Using different driving mechanisms at large scales, we have further shown that this scaling behavior is independent of the details of forcing. Moments of longitudinal and transverse velocity gradients, and those of dissipation and enstrophy, possess different sets of scaling exponents. In particular, the scaling exponents are larger for transverse gradients, consistent with the literature [13, 39, 41, 44]. All scaling exponents can be predicted by the theory [19] by knowing the transition

R_λ. In particular, the theory predicts that higher exponents will be obtained if the transition occurs at a lower R_λ. This is indeed what we observe.

Another interesting point is that the theory [20] relates velocity gradient exponents to those of structure functions in the inertial range. Note that all results here are for $1 \lesssim R_\lambda \lesssim 100$, which are lower than those needed for an inertial range to emerge [16]. Yet, the inertial
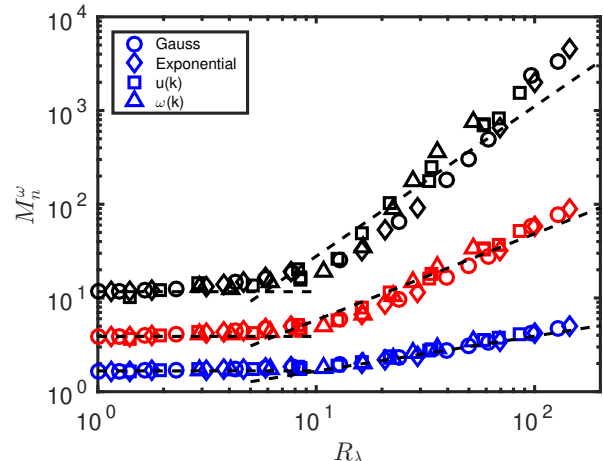

FIG. 4. Moments of enstrophy for $n = 2$ (blue), 3 (red), 4 (black). Horizontal lines correspond to moments of χ^2 distribution with 3 degrees of freedom. The power-laws corresponds to $\langle \epsilon^n \rangle / \langle \epsilon \rangle^n \propto R_\lambda^{d_n}$.

range exponents calculated from the exponents β_{2n}^q obtained here, using the theory, are close to those observed in simulations and experiments at high R_λ where an inertial range does exist. A potential implication is that *certain* high Reynolds features can be studied using data from well resolved DNS at low to moderate R_λ, and do not need very high R_λ. From a physical point of view, the inertial range anomalies are the result of intermittency at small scales which appear at low R_λ even without an inertial range. In this view, the inertial range emerges only as an intermediate constraint to match the Gaussian large scales with the anomalous dissipative scales.

Finally, we have evidence to support the present view in passive scalar advection and compressible turbulence [26, 45]—also for the Burgers equation that is studied, e.g., in Ref. [46]. These results will be reported elsewhere.

[1] A. N. Kolmogorov, Local structure of turbulence in an incompressible fluid for very large Reynolds numbers, Dokl. Akad. Nauk. SSSR **30**, 299 (1941).

[2] A. S. Monin and A. M. Yaglom, *Statistical Fluid Mechanics*, Vol. 2 (MIT Press, 1975).

[3] G. K. Batchelor, *The theory of homogeneous turbulence*

(Cambridge University Press, 1953).

[4] A. N. Kolmogorov, A refinement of previous hypotheses concerning the local structure of turbulence in a viscous incompressible fluid at high Reynolds number, J. Fluid Mech. **13**, 82 (1962).

[5] U. Frisch, *Turbulence* (Cambridge University Press, 1995).

[6] K. R. Sreenivasan and R. A. Antonia, The phenomenology of small-scale turbulence, Annu. Rev. Fluid Mech. **29**, 435 (1997).

[7] Z.-S. She and E. Leveque, Universal scaling laws in fully developed turbulence, Phys. Rev. Lett. **72**, 336 (1994).

[8] K. R. Sreenivasan and V. Yakhot, Dynamics of three-dimensional turbulence from Navier-Stokes equations, Phys. Rev. Fluids **6**, 104604 (2021).

[9] V. Yakhot, S. Orszag, S. Thangam, T. Gatski, and C. Speziale, Development of turbulence models for shear flows by a double expansion technique, Phys. Fluids A: Fluid Dyn. **4**, 1510 (1992).

[10] R. Benzi, S. Ciliberto, R. Tripiccione, C. Baudet, F. Massaioli, and S. Succi, Extended self-similarity in turbulent flows, Phys. Rev. E **48** (1993).

[11] R. Benzi, S. Ciliberto, C. Baudet, and G. Chavarria, On the scaling of three-dimensional homogeneous and isotropic turbulence, Phys. D **80**, 385 (1995).

[12] K. P. Iyer, K. R. Sreenivasan, and P. K. Yeung, Reynolds number scaling of velocity increments in isotropic turbulence, Phys. Rev. E **95** (2017).

[13] K. P. Iyer, K. R. Sreenivasan, and P. K. Yeung, Scaling exponents saturate in three-dimensional isotropic turbulence, Phys. Rev. Fluids **5**, 054605 (2020).

[14] Y. Tsuji, Intermittency effect on energy spectrum in high-reynolds number turbulence, Phys. Fluids **16** (2004).

[15] T. Ishihara, T. Gotoh, and Y. Kaneda, Study of high-Reynolds number isotropic turbulence by direct numerical simulation, Annu. Rev. Fluid Mech. **41**, 165 (2009).

[16] D. A. Donzis and K. R. Sreenivasan, The bottleneck effect and the Kolmogorov constant in isotropic turbulence, J. Fluid Mech. **657**, 171 (2010).

[17] S. Corrsin, On local isotropy in turbulent shear flows, NACA R&M **58B11** (1958).

[18] J. Schumacher, J. D. Scheel, D. Krasnov, D. A. Donzis, V. Yakhot, and K. R. Sreenivasan, Small-scale universality in fluid turbulence, Proc. Nat. Acad. Sci. **111**, 10961 (2014).

[19] V. Yakhot and D. A. Donzis, Emergence of multiscaling in a random-force stirred fluid, Phys. Rev. Lett. **119** (2017).

[20] V. Yakhot and D. A. Donzis, Anomalous exponents in strong turbulence, Phys. D: Nonlin. Phen. **384**, 12 (2018).

[21] J. Schumacher, K. R. Sreenivasan, and V. Yakhot, Asymptotic exponents from low-Reynolds-number flows, New J. Phys. **9** (2007).

[22] V. Yakhot and K. R. Sreenivasan, Anomalous scaling of structure functions and dynamic constraints on turbulence simulations, J. Stat. Phys. **121**, 823 (2005).

[23] S. Chen, K. R. Sreenivasan, M. Nelkin, and N. Cao, Refined similarity hypothesis for transverse structure functions in fluid turbulence, Phys. Rev. Lett. **79**, 2253 (1997).

[24] D. A. Donzis, P. K. Yeung, and K. R. Sreenivasan, Dissipation and enstrophy in isotropic turbulence: Resolution

effects and scaling in direct numerical simulations, Phys. Fluids **20**, 45108 (2008).

[25] T. Gotoh, D. Fukayama, and T. Nakano, Velocity field statistics in homogeneous steady turbulence obtained using a high-resolution direct numerical simulation, Phys. Fluids **14**, 1065 (2002).

[26] T. Gotoh and J. Yang, Transition of fluctuations from gaussian state to turbulent state, Phil. Trans. Royal Soc. A **380**, 20210097 (2022).

[27] J. D. Gibbon and C. R. Doering, Intermittency and regularity issues in 3d Navier-Stokes turbulence, Arch. Rat. Mech. & Anal. **177**, 115 (2005).

[28] J. T. Beale, T. Kato, and A. Majda, Remarks on the breakdown of smooth solutions for the 3-D Euler equations, Comm. Math. Phys. **94**, 61 (1984).

[29] P. K. Yeung, D. A. Donzis, and K. R. Sreenivasan, Dissipation, enstrophy and pressure statistics in turbulence simulations at high Reynolds numbers, J. Fluid Mech. **700**, 5 (2012).

[30] J. Schumacher, Sub-Kolmogorov-scale fluctuations in fluid turbulence, Euro. Phys. Lett. **80** (2007).

[31] S. Pandey and J. Schumacher, Reservoir computing model of two-dimensional turbulent convection, arXiv:2001.10280 [physics] (2020).

[32] V. Eswaran and S. B. Pope, An examination of forcing in direct numerical simulations of turbulence, Comp. & Fluids **16**, 257 (1988).

[33] M. F. Linkmann and A. Morozov, Sudden relaminarization and lifetimes in forced isotropic turbulence, Phys. Rev. Lett. (2015).

[34] W. D. Mccomb, A. Berera, S. R. Yoffe, and M. F. Linkmann, Energy transfer and dissipation in forced isotropic turbulence, Phys. Rev. E **91** (2015).

[35] H. Y. Shih, T. L. Hsieh, and N. Goldenfeld, Ecological collapse and the emergence of travelling waves at the onset of shear turbulence, Nat. Phys. **12**, 245 (2016).

[36] D. Barkley, B. Song, V. Mukund, G. Lemoult, M. Avila, and B. Hof, The rise of fully turbulent flow, Nature **526**, 550 (2015).

[37] R. S. Rogallo, Numerical experiments in homogeneous turbulence, NASA Tech. Memo. 81315 (1981).

[38] D. A. Donzis, *Scaling of turbulence and turbulent mixing using Terascale numerical simulations*, Ph.D. thesis (2007).

[39] P. K. Yeung, K. R. Sreenivasan, and S. B. Pope, Effects of finite spatial and temporal resolution in direct numerical simulations of incompressible isotropic turbulence, Phys. Rev. Fluids **3** (2018).

[40] D. Buaria, A. Pumir, E. Bodenschatz, and P. K. Yeung, Extreme velocity gradients in turbulent flows, New J. Phys. **21**, 043004 (2019).

[41] B. Dhruva, Y. Tsuji, and K. R. Sreenivasan, Transverse structure functions in high-Reynolds-number turbulence, Phys. Rev. E **56**, R4928 (1997).

[42] G. Stolovitzky, K. R. Sreenivasan, and A. Juneja, Scaling functions and scaling exponents in turbulence, Phys. Rev. E **48**, R3217 (1993).

[43] T. Watanabe and T. Gotoh, Inertial-range intermittency and accuracy of direct numerical simulation for turbulence and passive scalar turbulence, J. Fluid Mech. **590**, 117 (2007).

[44] P. K. Yeung, X. M. Zhai, and K. R. Sreenivasan, Extreme events in computational turbulence, Proc. Nat. Acad. Sci. **112** (2015).

[45] S. Khurshid, *Signatures of Fully Developed Turbulence and Their Emergence in Direct Numerical Simulations*, Ph.D. thesis (2021).

[46] J. Friedrich, G. Margazoglou, L. Biferale, and R. Grauer, Multiscale velocity correlations in turbulence and Burgers turbulence: Fusion rules, Markov processes in scale, and multifractal predictions, Phys. Rev. E **98** (2018).